Hindawi
Shock and Vibration
Volume 2021, Article ID 8861159, 13 pages
https://doi.org/10.1155/2021/8861159

Research Article

Motion Control of a 4WS4WD Path-Following Vehicle: Dynamics-Based Steering and Driving Models

Zhonghua Zhang,[1] **Caijin Yang**,[1] **Weihua Zhang**,[1] **Yanhai Xu**,[2] **Yiqiang Peng**,[2] **and Maoru Chi**[1]

[1]*State Key Laboratory of Traction Power, Southwest Jiaotong University, Chengdu 610031, China*
[2]*School of Transportation and Automotive Engineering, Xihua University, Chengdu 610039, China*

Correspondence should be addressed to Caijin Yang; ycj78_2012@163.com

Received 10 June 2020; Revised 31 October 2020; Accepted 19 December 2020; Published 16 January 2021

Academic Editor: Abdullah Seçgin

This paper deals with a four-wheel-steering four-wheel-driving (4WS4WD) vehicle under the path-following control. Focuses are placed on the motion control of the vehicle, and the drive forces and steering angles for achieving accurate path-following by the vehicle are determined. In this research, a nonlinear vehicle model of three degrees of freedom (DOFs) is used. The vehicle path-following dynamics are modeled using the classical mass-damper-spring vibration theory, which is described by three ordinary differential equations of second order with lateral, heading and velocity deviations, and control parameters. Combined with the vehicle path-following dynamic model, the nonlinear vehicle dynamic model is decoupled in generalized coordinate space. The required drive forces and steering angles for the vehicle path-following controllers are thus calculated and control models are obtained. Theoretical analysis for steering and driving control models is also carried out. It discloses that control models can maintain good performance against uncertainties. The vehicle path-following control is exhibited by dynamic simulation in CarSim with consideration of a complex vehicle model and a variable-curvature planned path. Numerical results obtained are analyzed and show control models have capable of dealing with a complex path-following problem. This paper provides a new insight into understanding path-following control of a 4WS4WD vehicle at the generalized vibration level.

1. Introduction

The demand for good acceleration and maneuvering performances of a road vehicle is ever increasing in the modern automotive industry. To meet this demand, novel vehicles such as four-wheel-steering (4WS) vehicles [1–4] and four-wheel-driving (4WD) vehicles [5–9] have thus been developed. Compared with conventional road vehicles, these vehicles are often equipped with multiple steering and/or driving devices so that they have the advantages of smaller turning radius, higher maneuverability, and better traction. During the past several years, the 4WS vehicles and 4WD vehicles have been received extensive researches and rich achievements are obtained. Li [1] proposed a new LVP control strategy with robustness for 4WS vehicles under velocity-varying motion. Chen [2] investigated nonlinear input-output decoupling control for 4WS vehicles with an observer. Marlene Kreutz [3] presented two design strategies for an active rear-wheel steering control system to improve the maneuverability and stability of four-wheel steering vehicles. In Ref. [5], Chen considered modeling errors and complex driving scenarios, and further studied the path-following control of autonomous four-wheel-independent-drive electric vehicles by means of second-order sliding mode and nonlinear disturbance observer techniques. Zhang [7] discussed the actuator fault detector design problem for an electric ground vehicle equipped with an active 4WS system. Nguyen [8] aimed at the shared lateral control between the human driver and lane-keeping assist system and developed a driver-automation cooperative control approach for intelligent vehicles that may be equipped with multiwheel steering and/or driving systems.

In Ref. [9], this researcher also investigated the path-following control problem of autonomous intelligent vehicles and proposed a fuzzy static output feedback control method.

In recent years, another promising vehicle has been received considerable attention from researchers and engineers, namely, the four-wheel-steering four-wheel-driving (4WS4WD) vehicles [10, 11] with excellent maneuverability and strong traction. The 4WS4WD vehicle is an over-actuated system where each of the four wheels can independently steer and drive. It can, therefore, combine with the benefits of 4WS vehicles and 4WD vehicles and have superiority over conventional road vehicles, 4WS vehicles, and 4WD vehicles in engineering applications. In particular, a 4WS4WD vehicle under the path-following control can be used to perform various tasks or missions. For example, a path-following vehicle is able to be an autonomous mobile carrier for heavy goods and human transportation. It can even carry out scientific research activities in outer space due to excellent performances and complex space conditions. Hence, it is of great significance for studying the path-following 4WS4WD vehicle, both theoretically and practically.

This paper deals with the path-following control of the 4WD4WS vehicle. This topic has been studied by some researchers and engineers. Representative studies could be found in the literature [12–23]. Majura F. [12] investigated the path-following control of ground robotic vehicles with four independently steered and driven wheels. Closed-loop kinematic constraints of the vehicle were established using the path geometry and the vehicle speed only. With established constraints, steering angles and speeds of individual wheels of the vehicle were determined, and then, a path-tracking controller was developed. Elie Maalouf [13] designed a fuzzy logic path-following controller for a wheeled-mobile robot. This controller is highly robust and flexible. Moreover, it can control the robot at a higher level and automatically follow a sequence of discrete waypoints. No interpolation of the waypoints was needed to generate a continuous reference trajectory in controller design. Martin Udengaard [14] presented a kinematic analysis and control method for an omnidirectional mobile robot, whose average isotropy was analyzed as a function of wheel module geometry on both flat and rough terrain. A simple kinematic controller with the effects of terrain unevenness was presented, and the performance of the presented algorithm was studied by simulation in Ref. [14]. Reza Oftadeh [15] provided a motion control law that can make the base follow a given smooth path and heading profile. This law was successfully used to solve the problem of motion control for a mobile robot with four individual steers and drive wheels.

Farbod Fahimi [16] proposed a 3DOFs dynamic model-based controller for four-wheel-steer and all-wheel-drive vehicles with consideration of considered parameter uncertainty. The controller proposed was capable of regulating longitudinal, lateral, and yaw motions of the vehicle simultaneously. Simulation results showed that the controller was robust. By integrating sliding mode control and particle swarm optimization, Dai [17] presented a novel control method for the path following a 4WS4WD vehicle. This control method had the ability to resist nonlinear, highly coupled and overactuated characteristics of the 4WS4WD vehicle. The robustness of this method was demonstrated by simulations. Liang [18] proposed a comprehensive control method for the 4WS4WD vehicle, which integrated active steering and direct yaw moment control systems. The proposed integrated control method can effectively improve the lateral dynamics performance of the vehicle at high speeds as compared to previous methods. Peng [19] presented an approach of wheel slip constraint to control an autonomous 4WS4WD vehicle. An integral compensation with a low-and-high gain technique was exploited to simultaneously eliminate the steady-state error of the path tracking and enhance the utilization of the constrained wheel slip. Simulation results showed that the proposed scheme was effective. Ramprasad Potluri [20] studied the path-tracking control of an autonomous 4WS4WD electric vehicle using its natural feedback loops. A trajectory tracking control scheme is developed for a four-wheel-independent steering and four-wheel-independent driving mobile robot by Yang [21], where both nonlinear kinematic control and dynamic sliding-mode control are designed. Lee [22] investigated the path-tracking problem for 4WS4WD electric vehicles with input constraints, actuator faults, and external resistance. A hybrid fault-tolerant control approach was proposed, which combines the linear-quadratic control method and the control Lyapunov function technique. This method can not only maintain the vehicle's tracking performance in spite of faults, input constraints, and external resistance but also reduce the cost of the fault-tolerant process. Li [23] investigated the path-tracking control problem of 4WS4WD road vehicles. An adaptive and fault-tolerant tracking control scheme was proposed in [23], which had capable of compensating vehicle uncertain dynamics/disturbances and actuation failures.

Though great efforts were made and some achievements were obtained in previous studies [12–23], the path-following control of the 4WS4WD vehicle may be worthy of further studying because of its complexity and unsolved problems. As well known, the 4WS4WD vehicle is an over-actuated system with six or eight control inputs. To maintain the good handling performance of the vehicle, all controls need to be accurate and cooperative at the high level. As for the path-following controllers [12–23] as concerned, some [12–15] are designed based on kinematic vehicle models while the others [16–23] are developed in vehicle dynamics. In general, kinematics-based control models [12–15] are simple and easy to be implemented. However, they are usually unable to afford dynamic disturbances and valid at low vehicle velocities. By contrast, dynamics-based control models [16–23] are often complex and may cause expensive computations despite that they are more accurate.

Motivated by mentioned-above problems, this paper aims at developing a dynamics-based method for fast determining steering angles and driving forces for achieving accurate path-following by a 4WS4WD vehicle. In this research, a 3DOFs nonlinear coupled dynamic model is used to describe the vehicle motions. The path-following problem of the vehicle is characterized using lateral, heading, and

velocity deviations. The mass-damper-spring model is adopted to form self-adaptive and self-stable zero-convergences of lateral, heading, and velocity deviations. The vehicle path-following dynamics are then modeled by three second-order ordinary differential equations of lateral, heading, and velocity deviations. Combined with the vehicle path-following dynamics model, the nonlinear motion model of the vehicle is decoupled by common approximation techniques. Linear equations with steering angles and driving forces of vehicle wheels are obtained and control input variables are thus determined. Compared with previous methods, the present method can maintain the main advantages of kinematics- and dynamics-based path-following control models. It is fast and robust with the nonlinear effects of vehicle dynamics. Original contributions of this paper are as follows: (1) the path-following dynamics of the vehicle are ascribed to the classical mass-damper-spring vibration problem. In this way, coupled nonlinear motion equations of the vehicle are successfully decoupled in generalized coordinate space. (2) A fast and robust method for determining all control input variables of a path-following 4WS4WD vehicle is proposed. The proposed method is analytical with nonlinear effects of vehicle dynamics and can be implemented in controllers without expensive computations. (3) Steering and driving control models of the vehicle obtained are examined and validated by means of dynamic simulation in CarSim with a complex vehicle model and planned path.

The rest part of this paper is organized as follows: after a brief description of a 4WS4WD vehicle system considered in Section 2, a 3DOFs nonlinear motion model of the vehicle is presented, and the vehicle path-following dynamics are modeled subsequently. The path-following problem is addressed using three uncoupled mass-damper-spring systems of single DOF with lateral, heading, and velocity deviations of the vehicle. In Section 3, a decoupling method is presented to determine steering angles and driving forces for the path-following vehicle from the nonlinear motion model of the vehicle. Important theoretical analysis for control models is carried out in this section. In Section 4, control models are examined and validated by using dynamic simulation in CarSim with consideration of a variable-curvature planned path and a complex vehicle model, instead of 3DOFs simple vehicle model used for the controller design. Dynamic results are obtained and analyzed. Conclusions are given finally.

2. Dynamic Modeling

A 4WS4WD vehicle system considered is shown in Figure 1. It is mainly composed of a vehicle body, four in-wheel motors, and two steering systems. Each motor can be driven independently. Each steering system consists of a steering servo motor and a mechanical device, which connects the wheels on the left and right sides of the vehicle. In this section, the modeling of the considered vehicle is presented first and the path-following dynamics of the vehicle are described next. Relevant details are provided below.

2.1. Vehicle Motion Model. For the sake of studying the motion control of the vehicle, the vehicle is routinely treated as a rigid body in a plane motion. Hence, the vehicle system can be modeled using three degrees of freedom represented by the coordinates X_C, Y_C, and θ. Note that the coordinates X_C, Y_C, and θ denote the X and Y components of displacement of the vehicle mass center and the yaw angle of the vehicle, respectively, which are defined in a global coordinate system OXY. Using Newton's second law of motion, motion equations of the vehicle can be established in terms of the mentioned-above coordinates. They are as follows:

the motion equation of the vehicle in the horizontal direction can be expressed as

$$m\ddot{X}_C = F_x\left(\delta_i, F_s^i, F_l^i, F_w, F_f, \theta\right), \tag{1}$$

where m is the mass of the vehicle and F_x is the resultant of all forces exerted on the vehicle along with the horizontal direction. In classical vehicle dynamics, the force F_x associates with the steering angle δ_i, the lateral force F_s^i, and the longitudinal force F_l^i of the ith wheel, in which a subscript $i = fl$, fr, rl, and rr, respectively, denotes the left and right wheels at front and rear axles of the vehicle, as well as the aerodynamic resistance F_w and the rolling resistance F_f of the vehicle. Note that these forces are formulated in the following text. The force F_x can be thus calculated as

$$F_x = f_x \cos\theta - f_y \sin\theta, \tag{2}$$

where the forces f_x and f_y are, respectively, defined as

$$f_x = F_l^f \cos\delta_f - F_s^f \sin\delta_f + F_l^r \cos\delta_r - F_s^r \sin\delta_r - F_w - F_f, \tag{3}$$

$$f_y = F_l^f \sin\delta_f + F_s^f \cos\delta_f + F_l^r \sin\delta_r + F_s^r \cos\delta_r, \tag{4}$$

in which there are [17]

$$\delta_f = \delta_{fl} = \delta_{fr}, \delta_r = \delta_{rl} = \delta_{rr}, \tag{5}$$

and

$$\begin{aligned} F_l^f &= F_l^{fl} + F_l^{fr}, \\ F_s^f &= F_s^{fl} + F_s^{fr}, \\ F_l^r &= F_l^{rl} + F_l^{rr}, \\ F_s^r &= F_s^{rl} + F_s^{rr}. \end{aligned} \tag{6}$$

Similarly, the motion equation of the vehicle in the vertical direction can be expressed as

$$m\ddot{Y}_C = F_y\left(\delta_i, F_s^i, F_l^i, F_w, F_f, \theta\right), \tag{7}$$

where F_y is the resultant of all forces exerted on the vehicle along with the vertical direction and can be defined as

$$F_y = f_x \sin\theta + f_y \cos\theta. \tag{8}$$

Moreover, the equation of the yaw motion of the vehicle can be expressed as

$$J\ddot{\theta} = M_z\left(\delta_i, F_s^i, F_l^i, F_w, F_f, \theta\right), \tag{9}$$

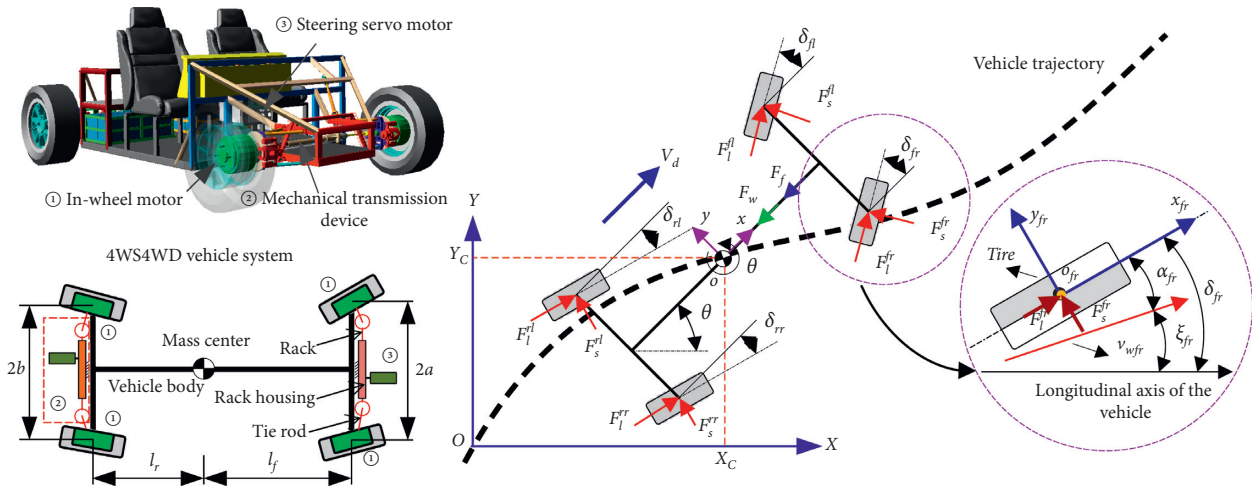

Figure 1: Schematic of a 4WS4WD vehicle system considered.

where J is the inertia moment of the yaw motion of the vehicle and the resultant moment M_z is defined as

$$M_z = \left(F_l^f \sin\delta_f + F_s^f \cos\delta_f\right)a + \left(F_l^r \sin\delta_r + F_s^r \cos\delta_r\right)b, \quad (10)$$

in which a and b denote half of the front and rear track widths, respectively.

For a general purpose, equations (1), (7), and (9) are rewritten in the matrix form as

$$\mathbf{M}\ddot{X} = \mathbf{F}, \quad (11)$$

where the coordinate vector $\mathbf{X} = [X_C, Y_C, \text{and } \theta]^T$, in which a superscript "T" denotes the transpose of a vector or matrix, and the mass matrix $\mathbf{M}$ and the force vector $\mathbf{F}$ are, respectively, expressed as

$$\mathbf{M} = \begin{bmatrix} m & 0 & 0 \\ 0 & m & 0 \\ 0 & 0 & J \end{bmatrix}, \quad (12)$$

$$\mathbf{F} = \begin{bmatrix} f_x \cos\theta - f_y \sin\theta \\ f_x \sin\theta + f_y \cos\theta \\ M_z \end{bmatrix}. \quad (13)$$

It is remarkably noted that the vehicle model in equation (11) is described in the global coordinate system OXY. It can be identical with the same one used in Ref. [16, 24] by means of a coordinate transformation.

2.1.1. Tire Model. The dynamic performance of a road vehicle largely depends on the characteristics of the tire. Various tire models are developed for the vehicle dynamics analysis and available in the literature, e.g., simple linear model [16–18, 24, 25] and complex magic formula [26, 27]. A classical linear tire model [16, 17] is adopted here for controller design routinely. In Refs. [18, 24], the lateral force F_s of the tire is calculated as

$$F_s = C_\alpha \alpha, \quad (14)$$

where C_α is the cornering stiffness of the tire and α is the slip angle of the tire. According to classical tire dynamics, the slip angle α is defined as

$$\alpha = \zeta - \delta, \quad (15)$$

where δ is the tire steering angle and ζ is the tire velocity angle. The tire velocity angle ζ is expressed as

$$\zeta = \tan^{-1}\left(\frac{v_y}{v_x}\right), \quad (16)$$

where v_x and v_y are two components of the velocity of the wheel center defined in the vehicle-body coordinate system oxy.

2.1.2. Resistances to the Vehicle Motion. The aerodynamic and rolling resistances are included in the vehicle model. In general, the aerodynamic resistance F_w depends on the air density ρ, the drag coefficient C_d, the frontal cross-sectional area A of the vehicle, and the longitudinal velocity V_d of the vehicle. In Refs. [1, 16, 24, 28], the aerodynamic resistance F_w is calculated as

$$F_w = C_d A \rho V_d^2. \quad (17)$$

Rolling resistance mainly results from tire deformation. The tire rolling resistance F_f can be simply calculated as [28, 29]

$$F_f = C_f mg, \quad (18)$$

where C_f is the rolling drag coefficient and g is the gravitational acceleration constant.

2.2. Vehicle Path-Following Dynamics. Sometimes, the vehicle is expected to follow a planned path. But, it inevitably deviates from the planned path due to some reasons, e.g., road disturbances. In this section, the vehicle path-following problem is addressed based on vehicle deviation dynamics together with the classical mass-damper-spring model. Important details are presented below.

2.2.1. Vehicle Path-Following Deviations. The path-following deviations of the vehicle in the current state from its

desired state can be measured using the lateral deviation ε_d, the heading deviation ε_θ, and the velocity deviation ε_v, as illustrated in Figure 2. The lateral deviation ε_d is defined as a minimal distance from a control point in the vehicle, e.g., the mass center C, to the planned path. The heading deviation ε_θ actually represents the angle between the vehicle centerline and the road tangent line. The velocity deviation ε_v is a difference between the instantaneous and planned velocities of the vehicle in the vehicle longitudinal direction.

2.2.2. Vehicle Deviation Dynamics. There is no doubt that the vehicle is in a state of three zero-deviations defined above when it accurately follows the planned path as expected. In that sense, the path-following of the vehicle is such a process that three-vehicle deviations converge zeros. Zero-convergence dynamics of lateral, heading, and velocity deviations of the vehicle are characterized in the following text.

Take zero-convergence dynamics of the vehicle lateral deviation as an example for illustrative purposes. Considering the mass-damper-spring model in classical vibration theory, the zero-convergence of the vehicle lateral deviation ε_d can be governed by

$$\ddot{\varepsilon}_d + c_d\dot{\varepsilon}_d + k_d\varepsilon_d = 0, \tag{19}$$

where constants c_d and k_d are control parameters introduced. It is obvious that nonzero lateral deviation ε_d in the system of equation (19) can quickly converge to nearly zero in classical vibration theory. In a similar way, zero-convergence dynamics for the vehicle heading and velocity deviations are addressed as

$$\ddot{\varepsilon}_\theta + c_\theta\dot{\varepsilon}_\theta + k_\theta\varepsilon_\theta = 0, \tag{20}$$

$$\dot{\varepsilon}_v + c_v\varepsilon_v = 0, \tag{21}$$

where constants c_θ, k_θ, and c_v are control parameters.

Next, equations (19)–(21) are rewritten in terms of vehicle coordinates. Considering a smooth planned path,

$$\varphi(X, Y) = 0, \tag{22}$$

where the curve φ is assumed to be continuous and differentiable to at least second order and knowing the vehicle state at any time, the deviations ε_d, ε_θ, and ε_v can be specified as follows. Let P be the projection point of the mass center C onto the curve φ. Without loss of generality, the position (X_P and Y_P) of point P can be expressed in an implicit form as

$$\begin{cases} X_P = \overline{f}(X_C, Y_C), \\ Y_P = \overline{g}(X_C, Y_C), \end{cases} \tag{23}$$

where the functions $\overline{f}$ and $\overline{g}$ are relation to the curve φ and the mass center C (X_C and Y_C). In terms of the differential geometry theory, the normal vector $\mathbf{n}$ and the tangential vector τ of the curve at projection point P (X_P, Y_P) are, respectively, expressed as

$$\mathbf{n} = [\varphi_X, \varphi_Y]^T, \tag{24}$$

$$\boldsymbol{\tau} = [-\varphi_Y, \varphi_X]^T, \tag{25}$$

where φ_X and φ_Y denote partial derivatives of the equation of the curve φ with respect to coordinates X and Y, respectively. The normalization of equation (25) leads to

$$\mathbf{n}_\tau = \frac{\boldsymbol{\tau}}{\|\boldsymbol{\tau}\|} = \frac{1}{\sqrt{\varphi_X^2 + \varphi_Y^2}}[-\varphi_Y, \varphi_X]^T, \tag{26}$$

where $\mathbf{n}_\tau$ is an unit vector. Let $\mathbf{h}$ be a unit vector that indicates the longitudinal direction of the vehicle. Considering the definition of the vehicle yaw angle θ, the unit vector $\mathbf{h}$ is then given as

$$\mathbf{h} = [\cos\theta, \sin\theta]^T. \tag{27}$$

Let V_d and V_t be the instantaneous and planned velocities of the vehicle in the longitudinal direction, respectively. The longitudinal velocity V_d can be expressed as

$$V_d = \dot{X}_C\cos\theta + \dot{Y}_C\sin\theta. \tag{28}$$

Thus, the lateral deviation, the heading deviation, and the velocity deviation are, respectively, given by

$$\varepsilon_d = \sqrt{(X_C - X_P)^2 + (Y_C - Y_P)^2} = f_d(X_C, Y_C, \theta), \tag{29}$$

$$\varepsilon_\theta = \cos^{-1}\left(\mathbf{h}^T\mathbf{n}_\tau\right) = f_\theta(X_C, Y_C, \theta), \tag{30}$$

$$\varepsilon_v = V_d - V_t = \dot{X}_C\cos\theta + \dot{Y}_C\sin\theta - V_t = f_v\left(\dot{X}_C, \dot{Y}_C, \theta, t\right). \tag{31}$$

Substituting equations (29)–(31) into equations (19)–(21) and rearranging them in terms of vehicle coordinates X_C, Y_C, and θ, the vehicle path-following dynamics can be described as

$$\overline{M}\ddot{X} = \overline{F}, \tag{32}$$

where the matrix $\overline{M}$ is defined as

$$\overline{M} = \begin{bmatrix} \dfrac{\partial f_v}{\partial \dot{X}_C} & \dfrac{\partial f_v}{\partial \dot{Y}_C} & 0 \\ \dfrac{\partial f_d}{\partial X_C} & \dfrac{\partial f_d}{\partial Y_C} & \dfrac{\partial f_d}{\partial \theta} \\ \dfrac{\partial f_\theta}{\partial X_C} & \dfrac{\partial f_\theta}{\partial Y_C} & \dfrac{\partial f_\theta}{\partial \theta} \end{bmatrix}, \tag{33}$$

and the force vector $\overline{F}$ is defined as

$$\overline{F} = -\begin{bmatrix} \dfrac{\partial f_v}{\partial \theta}\dot{\theta} + c_v\varepsilon_v + \dot{V}_t \\ \dot{X}^T\mathbf{H}_d\dot{X} + c_d\dot{\varepsilon}_d + k_d\varepsilon_d \\ \dot{X}^T\mathbf{H}_\theta\dot{X} + c_\theta\dot{\varepsilon}_\theta + k_\theta\varepsilon_\theta \end{bmatrix}, \tag{34}$$

in which $\mathbf{H}_d$ and $\mathbf{H}_\theta$, respectively, have forms of

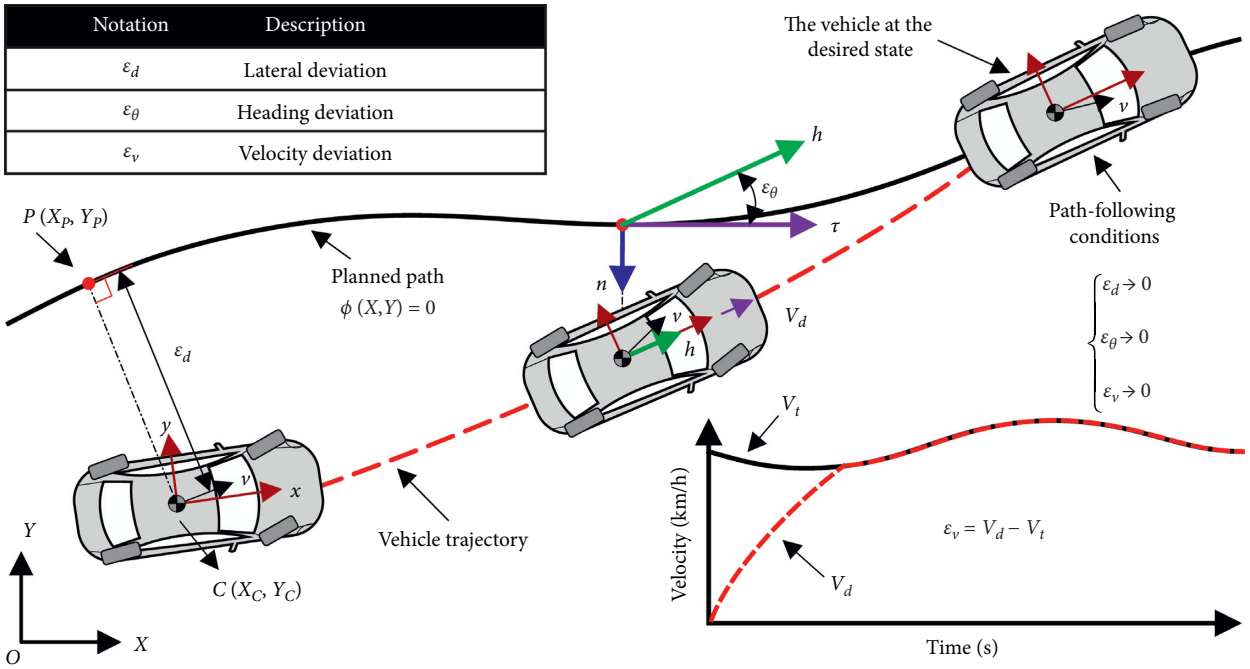

Figure 2: Path following deviations of the vehicle in current state from its desired state.

$$\mathbf{H}_d = \begin{bmatrix} \frac{\partial^2 f_d}{\partial X_C^2} & \frac{\partial^2 f_d}{\partial Y_C \partial X_C} & \frac{\partial^2 f_d}{\partial \theta \partial X_C} \\ \frac{\partial^2 f_d}{\partial X_C \partial Y_C} & \frac{\partial^2 f_d}{\partial Y_C^2} & \frac{\partial^2 f_d}{\partial \theta \partial Y_C} \\ \frac{\partial^2 f_d}{\partial X_C \partial \theta} & \frac{\partial^2 f_d}{\partial Y_C \partial \theta} & \frac{\partial^2 f_d}{\partial \theta^2} \end{bmatrix}, \quad \mathbf{H}_\theta = \begin{bmatrix} \frac{\partial^2 f_\theta}{\partial X_C^2} & \frac{\partial^2 f_\theta}{\partial Y_C \partial X_C} & \frac{\partial^2 f_\theta}{\partial \theta \partial X_C} \\ \frac{\partial^2 f_\theta}{\partial X_C \partial Y_C} & \frac{\partial^2 f_\theta}{\partial Y_C^2} & \frac{\partial^2 f_\theta}{\partial \theta \partial Y_C} \\ \frac{\partial^2 f_\theta}{\partial X_C \partial \theta} & \frac{\partial^2 f_\theta}{\partial Y_C \partial \theta} & \frac{\partial^2 f_\theta}{\partial \theta^2} \end{bmatrix}. \tag{35}$$

3. Steering and Driving Control Models

The current vehicle system steers by two servo motors and drives by four in-wheel motors. There are, therefore, six control inputs and redundant controls exist. For the sake of simplicity, it is assumed that longitudinal forces of tires on the front and rear vehicle axes have a proportional relationship of the constant ratio k_{fr}. The following equation is then obtained as

$$F_l^f = k_{fr} F_l^r. \tag{36}$$

Thus, four control inputs are required in the vehicle motion control. They are steering angles δ_f and δ_r and longitudinal tire forces F_l^f and F_l^r. A decoupling method is presented below to determine these control variables from the nonlinear vehicle model in equation (11).

3.1. Dynamic Decoupling and Determination of Control Inputs. Multiplying equation (12) by an inverse matrix $\mathbf{M}^{-1}$ leads to

$$\ddot{X} = \mathbf{M}^{-1}\mathbf{F}. \tag{37}$$

Substituting equation (37) into equation (32) yields

$$\overline{M}\mathbf{M}^{-1}\mathbf{F} = \overline{F}. \tag{38}$$

Equation (32) is useful in the sense that it provides dynamic constraints on control input variables. The combination of equation (36) with equation (38) leads to

$$\mathbf{A}\mathbf{x} = \mathbf{b}, \tag{39}$$

where $\mathbf{x} = [F_l^f, \delta_f, F_l^r, \delta_r]^T$ and a four by four matrix $\mathbf{A}$ is expressed as

$$\mathbf{A} = \begin{bmatrix} \cos\theta\cos\delta_f - \sin\theta\sin\delta_f & \cos\theta C_\alpha^f \sin\delta_f + \sin\theta C_\alpha^f \cos\delta_f & \cos\theta\cos\delta_r - \sin\theta\sin\delta_r & \cos\theta C_\alpha^r \sin\delta_r + \sin\theta C_\alpha^r \cos\delta_r \\ \sin\theta\cos\delta_f + \cos\theta\sin\delta_f & \sin\theta C_\alpha^f \sin\delta_f - \cos\theta C_\alpha^f \cos\delta_f & \sin\theta\cos\delta_r + \cos\theta\sin\delta_r & \sin\theta C_\alpha^r \sin\delta_r - \cos\theta C_\alpha^r \cos\delta_r \\ l_f \sin\delta_f & -l_f C_\alpha^f \cos\delta_f & -l_r \sin\delta_r & l_r C_\alpha^r \cos\delta_r \\ 1 & 0 & -k_{fr} & 0 \end{bmatrix} \tag{40}$$

and the four by one vector $\mathbf{b}$ is expressed as

$$\mathbf{b} = \begin{bmatrix} \left(\begin{array}{c} \cos\theta C_\alpha^f \zeta_f \sin\delta_f + \sin\theta C_\alpha^f \zeta_f \cos\delta_f + \cos\theta C_\alpha^r \zeta_r \sin\delta_r \\ +\sin\theta C_\alpha^r \zeta_r \cos\delta_r + \cos\theta\left(F_w + F_f\right) \end{array} \right) \\ \left(\begin{array}{c} \sin\theta C_\alpha^f \zeta_f \sin\delta_f - \cos\theta C_\alpha^f \zeta_f \cos\delta_f + \sin\theta C_\alpha^r \zeta_r \sin\delta_r \\ -\cos\theta C_\alpha^r \zeta_r \cos\delta_r + \left(F_w + F_f\right)\sin\theta \end{array} \right) \\ -l_f C_\alpha^f \zeta_f \cos\delta_f + l_r C_\alpha^r \zeta_r \cos\delta_r \\ 0 \end{bmatrix} + \begin{bmatrix} \boldsymbol{\eta} \\ 0 \end{bmatrix}, \tag{41}$$

in which the three by one vector η has the form of

$$\boldsymbol{\eta} = \mathbf{M}\overline{M}^{-1}\overline{F}, \tag{42}$$

where $\overline{M}^{-1}$ is the inverse matrix of $\overline{M}$.

It is importantly noted that matrix $\mathbf{A}$ is highly nonlinear and is relation to the yaw angle θ, steering angles δ_f and δ_r, and tire velocity angles ζ_f and ζ_r, as well as constants C_α^f, C_α^r, a,b, and k_{fr}. The yaw angle θ at each time step can be determined by the sensor measurement. For a small sample of time, steering angles δ_f and δ_r at the current time step can be approximated by those at a previous time step in controller design. In this way, the matrix $\mathbf{A}$ can be calculated in equation (40) without effort. Similarly, the vector $\mathbf{b}$ can be calculated in equation (41) at the current time step. Control input variables $\mathbf{x}$ at the current time step are thus determined as

$$\mathbf{x} = \mathbf{A}^{-1}\mathbf{b}, \tag{43}$$

where $\mathbf{A}^{-1}$ is the inverse matrix of matrix $\mathbf{A}$. Note that the inverse matrix of matrix $\mathbf{A}$ does not exist in the case that the vehicle heads towards the tangent of the path curve. Singular problems in current control models will be discussed in other research, for the sake of conciseness. Knowing the above variables, other variables in motor controllers can be determined. For example, the motor driving or braking torque is used as control input in some controllers. For this case, they can be obtained in Refs. [18, 21].

Now, steering and driving control models in equation (43) are understood. Since equation (43) results from the vehicle motion model in equation (11) and the vehicle path-following dynamic model in equation (32), control models in this research inherit main properties from both the vehicle model and vehicle path-following model. It means that equation (43) builds a bridge between vehicle dynamics and vehicle path-following dynamics. Clearly, the vehicle dynamics in equation (11) are nonlinearly coupled with control variables in physical coordinate space while the vehicle path-following dynamics in equation (19)–(21) or equation (32) are uncoupled in generalized coordinate space of ε_d, ε_θ, and ε_v. In that sense, the vehicle physical motions can be projected and decoupled in a generalized coordinate space. Thus, steering angles and driving forces of all wheels for achieving the path-following of the vehicle can be determined from the coupled vehicle dynamic model in this way. Moreover, the inverse matrix $\mathbf{A}^{-1}$ can be analytically expressed with the analysis of matrix A. Thus, the four-dimensional linear equations, namely, equation (43), have the analytical expression. In other words, control input variables can be fast determined in equation (43).

3.2. Theoretical Analysis and Discussion on Control Models. As described above, some approximations are taken into account to determine control input variables, e.g., the approximation of matrix $\mathbf{A}$ in equation (40) at the previous time step. Here, the effects of approximations taken on the vehicle path-following control are analyzed.

Corresponding problems caused by approximations taken are solved by the perturbation analysis of equations (19)–(21). To perform the analysis, equation (11) is rewritten to

$$\mathbf{M}\ddot{X} = \mathbf{F} + \Delta\mathbf{F}, \tag{44}$$

where $\Delta\mathbf{F}$ denotes an increment caused by approximations taken. Thus, the acceleration term $\ddot{X}$ is obtained from equation (44) as

$$\ddot{X} = \mathbf{M}^{-1}\mathbf{F} + \mathbf{M}^{-1}\Delta\mathbf{F}. \tag{45}$$

Considering equation (45), the perturbation of equation (32) reads

$$(\overline{M} + \Delta\overline{M})\left(\mathbf{M}^{-1}\mathbf{F} + \mathbf{M}^{-1}\Delta\mathbf{F}\right) - (\overline{F} + \Delta\overline{F}) = \overline{M}\mathbf{M}^{-1}\mathbf{F} - \overline{F} + \Delta\widetilde{F} = \overline{M}\ddot{X} - \overline{F} + \Delta\widetilde{F} = 0. \tag{46}$$

where $\Delta\overline{M}$ and $\Delta\overline{F}$ are dynamic terms caused by approximations taken, and the perturbation term $\Delta\widetilde{F}$ is defined as

$$\Delta\widetilde{F} = \overline{M}\mathbf{M}^{-1}\Delta\mathbf{F} + \Delta\overline{M}\left(\mathbf{M}^{-1}\mathbf{F} + \mathbf{M}^{-1}\Delta\mathbf{F}\right) - \Delta\overline{F}. \tag{47}$$

By contrast with equations (19)–(21), the separation of equation (46) leads to

$$\ddot{\varepsilon}_d + c_d\dot{\varepsilon}_d + k_d\varepsilon_d + \Delta f_d = 0, \tag{48}$$

$$\ddot{\varepsilon}_\theta + c_\theta\dot{\varepsilon}_\theta + k_\theta\varepsilon_\theta + \Delta f_\theta = 0, \tag{49}$$

$$\dot{\varepsilon}_v + c_v\varepsilon_v + \Delta f_v = 0, \tag{50}$$

where Δf_d, Δf_θ, and Δf_v are nonlinear functions of ε_d, ε_θ, and ε_v, as well as parameters and variables mentioned above. In the classical vibration theory, lateral, heading, and velocity deviations govern by equations. (48)–(50) may converge to nonzero constant values $\widehat{\varepsilon}_d$, $\widehat{\varepsilon}_\theta$, and $\widehat{\varepsilon}_v$ at the steady state. The values $\widehat{\varepsilon}_d$, $\widehat{\varepsilon}_\theta$, and $\widehat{\varepsilon}_v$ can be calculated as

$$k_d\widehat{\varepsilon}_d + \Delta f_d = 0, \tag{51}$$

$$k_\theta\widehat{\varepsilon}_\theta + \Delta f_\theta = 0, \tag{52}$$

$$c_v\widehat{\varepsilon}_v + \Delta f_v = 0. \tag{53}$$

Based on the above analysis, it can be concluded that current control models have capable of achieving the path-following motion of the vehicle against approximations taken. However, the approximations taken have an active influence on the vehicle path-following accuracy.

Equations (48)–(53) are reconsidered and further analyzed. The analysis may discover that the path-following accuracy of the vehicle can be improved by means of adjusting control parameters. For illustration purpose, the vehicle is assumed to be in a stable state that it laterally deviates from a planned path. A simple and feasible method for improving the path-following accuracy of the vehicle is presented here according to equation (51). Without loss of generality, the term Δf_d in equation (51) can be written as

$$\Delta f_d = \Delta k_d\varepsilon_d - O_d, \tag{54}$$

where Δk_d can be a constant and the truncation error O_d is close to zero. Substituting equation (54) into equation (48) yields

$$\ddot{\varepsilon}_d + c_d\dot{\varepsilon}_d + (k_d + \Delta k_d)\varepsilon_d = O_d \approx 0. \tag{55}$$

It is thus concluded from equation (55) that the path-following accuracy of the vehicle can be improved by proper control parameter $k_d + \Delta k_d$, to some extent. By considering equations (52) and (53), similar conclusions are obtained. Importantly note that dynamic term $\Delta k_d\varepsilon_d$ is caused by many reasons, e.g., unknown road conditions, inaccuracy of vehicle and tire models used, and even some uncertainties. In that sense, current control models are robust and effective against uncertainties.

4. Model Validation and Dynamic Results

Steering and driving control models in equation (43) are examined by dynamic simulation in this section. The vehicle system shown in Figure 1 is modeled in CarSim using simulation parameters listed in Table 1. A variable-curvature path is considered and illustrated in Figure 3. As shown in Figure 3, the planned path is composed of line-straight segments and circular segments.

In simulation, control parameters are taken as: $c_d = 15.0$, $k_d = 5.0$, $c_\theta = 15.0$, $k_\theta = 5.0$, and $c_v = 1.5$. The vehicle is initially at rest and deviates from the path with a lateral distance of 0.5 m. After starting, the vehicle experiences four distinct stages. In the first stage, the longitudinal velocity of the vehicle increases from zero to 5.0 m/s with a constant acceleration of 1.0 m/s^2. Then, the longitudinal velocity of the vehicle maintains constantly in the second stage. After simulation time $t = 30$ s, the longitudinal velocity of the vehicle decreases up to 3.0 m/s with the acceleration of -1.0 m/s^2 in the third stage. In the last stage, the vehicle runs along the path at another constant velocity of 3.0 m/s. Under the above conditions, the path-following dynamics of the vehicle are simulated. Dynamic results are obtained and presented below.

Figure 4 shows time-domain variations of lateral, heading, and velocity deviations of the vehicle under the path-following control. Figure 5 shows comparisons of the trajectory of the vehicle controlled with the planned path. It can be seen in Figures 4 and 5 that control models take effect at the higher level. The vehicle controlled quickly enters into the planned path and then better runs along the path against with discontinuous curvature variations of the path. The maximum lateral deviation is about 0.077 m, the maximum heading deviation is about 13 degrees, and the maximum velocity deviation is about 1.0 km/h. As observed in Figure 5, the vehicle path-following deviations may fluctuate slightly as the vehicle enters into or leaves off the straight-curved/curved-straight sections of the path. This phenomenon is caused by discontinuous variations of the path curvature at these regions. Control models are free from these fluctuations and continuously effective.

Figure 6 shows time-domain variations of steering angles of wheels and longitudinal forces of tires of the vehicle controlled. From the curves plotted in Figure 6(a), one can see that the vehicle initially turns in such a way that all wheels steer towards the same direction. Thus, the initial lateral deviation of the vehicle can be quickly diminished. By contrast, the rear wheels steer the opposite direction of the front wheels in the case that the vehicle stably runs along the circular sections of the path. There are two distinct steering modes. The phenomena show that control models are able to autonomously determine steering modes to fit into various circumstances. It just demonstrates the excellent maneuvering performance of the 4WS4WD vehicle. Moreover, it is interesting to note that steering angles of the front and rear wheels reversely vary with a decrease of the curvature

Table 1: Vehicle parameters used in simulation.

Notation	Value	Unit
Vehicle mass m	1060	Kg
Inertia moment J	1523	kg·m^2
Cornering stiffness of front tire $Cf\ \alpha$	−61060	N/rad
Cornering stiffness of rear tire $Cr\ \alpha$	−97920	N/rad
Half of front track width a	0.79	M
Half of rear track width b	0.84	M
The distance from mass center of vehicle to front axles l_f	1.539	M
The distance from mass center of vehicle to rear axles l_r	1.539	M
Air density ρ	1.2258	N/s^2/m^4
Air drag coefficient C_d	0.3	—
Frontal cross-sectional area A	2.5	m^2
Tire rolling resistance C_f	0.01	—
Gravitational constant g	9.8	m/s^2
Friction coefficient μ	0.8	—

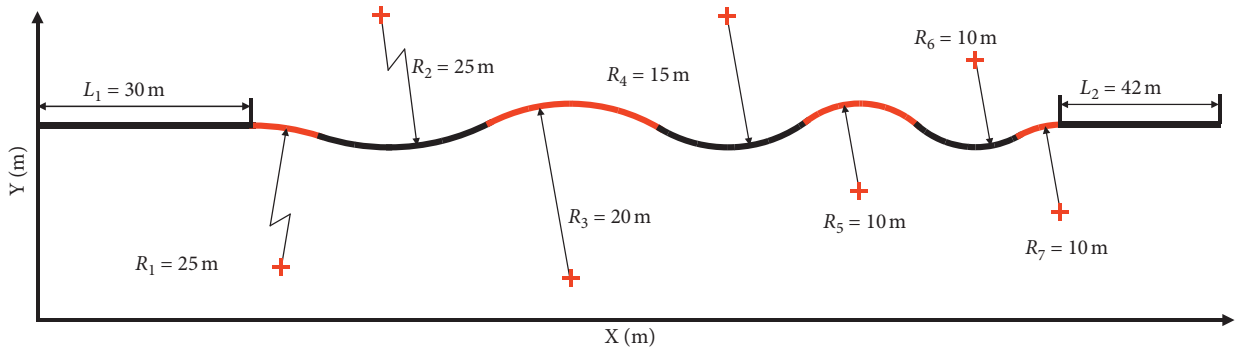

Figure 3: Schematic of the planned path.

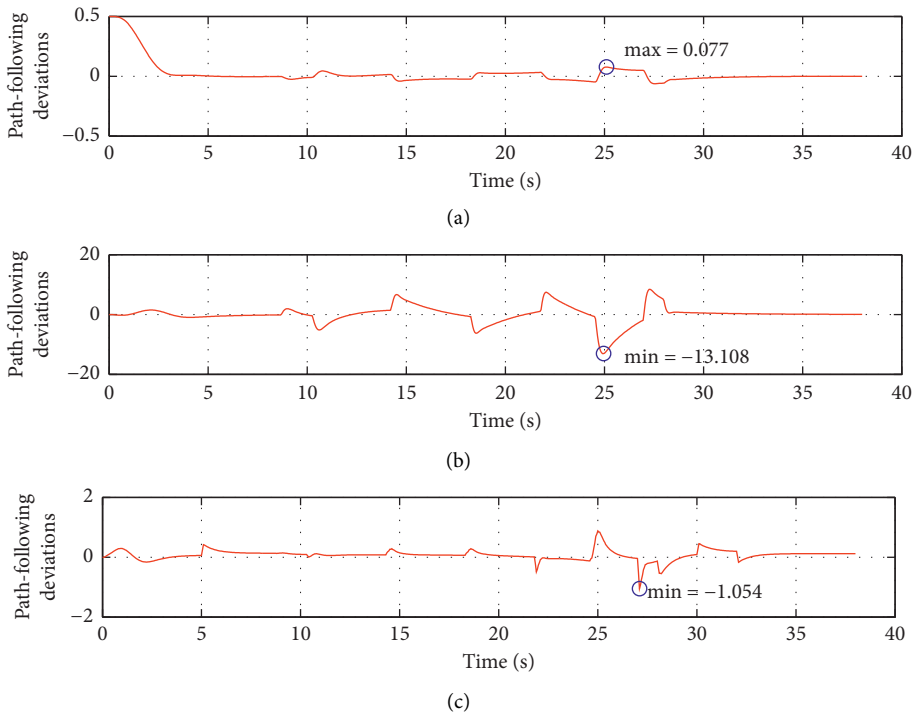

Figure 4: Time histories of path-following deviations of the vehicle under control. (a) Lateral deviation (m). (b) Heading deviation (deg). (c) Velocity deviation (km/h).

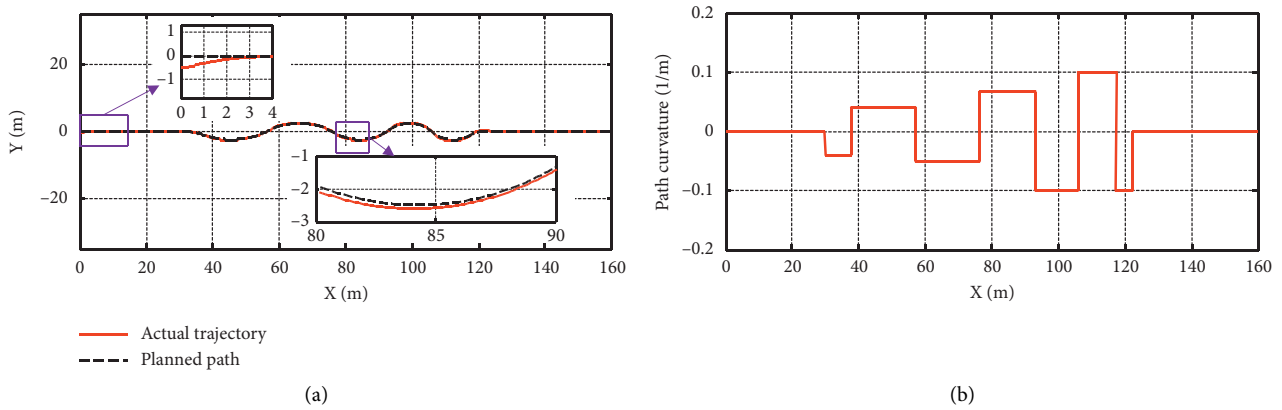

Figure 5: The trajectory of the path-following vehicle against curvature variations of the path.

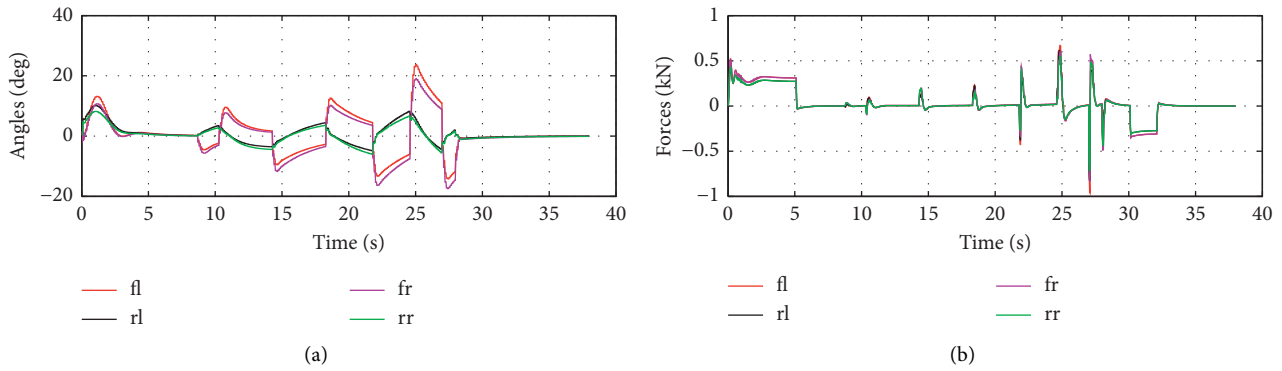

Figure 6: Time histories for steering angles of wheels and longitudinal forces of tires during the vehicle path-following control. (a) Wheel steering angle. (b) Longitudinal force of tire.

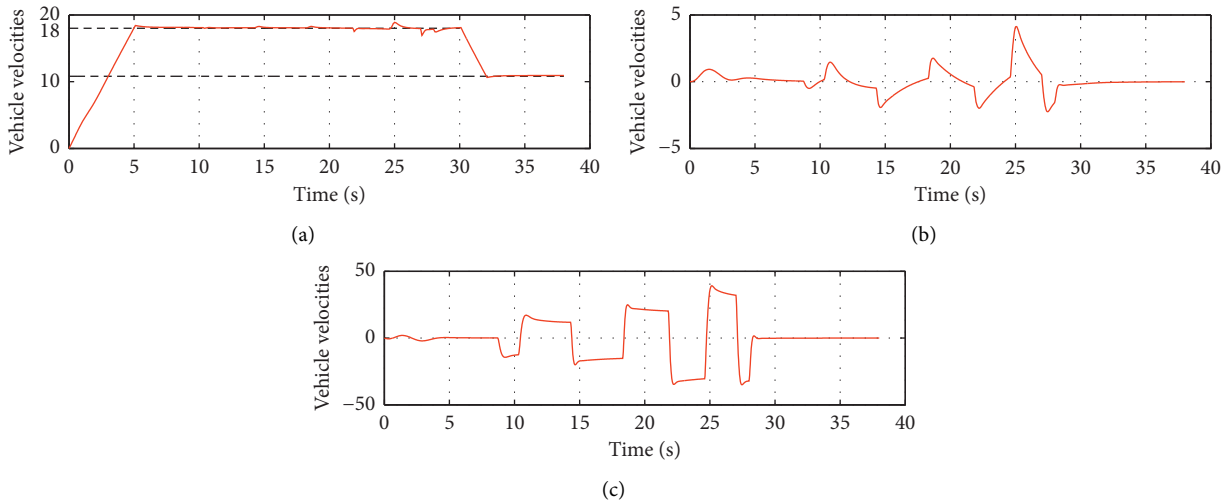

Figure 7: Time histories for longitudinal and lateral velocities and yaw rate of the path-following vehicle. (a) Longitudinal velocity (km/h). (b) Lateral velocity (km/h). (c) Yaw velocity (deg/s).

radius of the path as the vehicle is stable in circular sections of the path. It can be understood in this sense that larger lateral forces of the vehicle are required as it runs along the circular path with a smaller radius at the same velocity, corresponding to larger steering angles of wheels. Figure 6(b) shows several jumps in the curves of longitudinal forces of tires. As observed in Figure 6(b), these jumps mainly arise in the locations where the

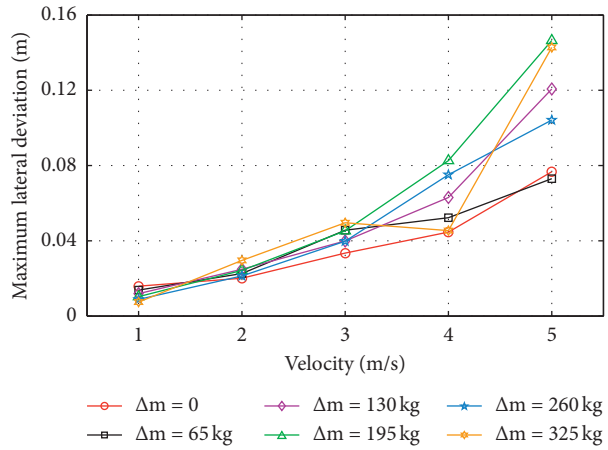

Figure 8: Variations of maximum lateral deviation of the vehicle controlled against vehicle mass under different vehicle velocities.

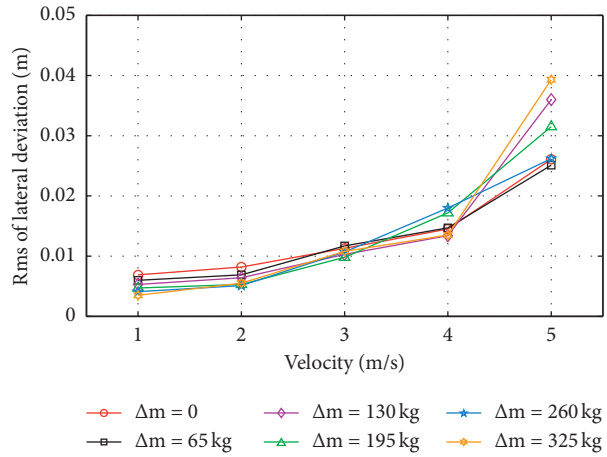

Figure 9: Variations of root mean square of lateral deviation of the vehicle controlled against vehicle mass under different vehicle velocities.

vehicle is near straight-curved/curved-straight sections of the path. Thus, it can be included that these jumps are caused by discontinuous curvature variations of the path in the above locations. Figure 7 shows time-domain responses of longitudinal and lateral velocities and yaw rate of the vehicle controlled. As clearly shown in Figure 7(a), the vehicle controlled runs along the path with the desired velocities as expected.

Steering and driving control models are further examined by considering variations of vehicle mass with an increment of 65 kg. Figure 8 shows the change of maximum lateral deviation of the vehicle with vehicle mass under different velocities. It can be seen in Figure 8 that there is a trend towards an increased maximum lateral deviation of one vehicle with the larger longitudinal velocity of the vehicle. Moreover, the maximum lateral deviation may become larger with an increase of vehicle mass in the case of a certain longitudinal velocity of the vehicle. Similar phenomena are found in the curves plotted in Figure 9. Figure 9 shows the variations of root mean square of lateral deviation of the vehicle against vehicle mass under different vehicle velocities. From Figures 8 and 9, one can conclude that the control models of this paper are robust, to some extent [30].

5. Conclusions

The path-following motion control of a 4WS4WD vehicle is studied. A fast and robust method is developed to determine control input variables for achieving an accurate path-following of the vehicle. Steering and driving control models are validated both theoretically and numerically. Important results obtained are as follows:

(1) Motion controls of the path-following vehicle can be regarded as such a process that three deviations

converge to zeros. The vehicle path-following dynamics can be modeled using the classical mass-damper-spring vibration theory and characterized by three second-order ordinary differential equations of parameters k_d, c_d, k_d, c_θ, and c_v.

(2) Control models of this paper have good quality. Theoretical analysis shows that control models are effective against uncertainties. Numerical studies show that control models still take effect and afford to a complex path-following problem in Sect. 4.

Data Availability

The figure and table of simulation results used to support the findings of this study are included within the article.

Conflicts of Interest

The authors declare that they have no conflicts of interest.

Acknowledgments

The authors would like to thank supports from the National Natural Science Foundation of China (Grant no. 51775448), the Project for Innovation Talents of Science and Technology of Sichuan Province (no. 2020JDRC0008), the Key Research Project of Sichuan Science and Technology Program (no. 2020YFG0023), the Applied Basic Research Programs of Sichuan Province (no. 2018JY0557), the Chengdu Technological Innovation R & D Project (No. 2018-YF05-00813-SN), the Project of State Key Laboratory of Traction Power for Southwest Jiaotong University (no. 2016TPL_Z01), the Open Research Subject of Key Laboratory for Xihua University (no. SZJJ2015-049), and the Fundamental Research Funds for the Central Universities (no. 2682018CX70).

References

[1] M. Li, Y. Jia, and J. Du, "LPV control with decoupling performance of 4WS vehicles under velocity-varying motion," *IEEE Transactions on Control Systems Technology*, vol. 22, no. 5, pp. 1708–1724, 2014.

[2] C. Chen and Y. Jia, "Nonlinear decoupling control of four-wheel-steering vehicles with an observer," *International Journal of Control, Automation and Systems*, vol. 10, no. 4, pp. 697–702, 2012.

[3] M. Kreutz, M. Horn, and J. Zehetner, "Improving vehicle dynamics by active rear wheel steering systems," *Vehicle System Dynamics*, vol. 47, no. 12, pp. 1551–1564, 2009.

[4] T. Hiraoka, O. Nishihara, and H. Kumamoto, "Automatic path-tracking controller of a four-wheel steering vehicle," *Vehicle System Dynamics*, vol. 47, no. 10, pp. 1205–1227, 2009.

[5] J. Chen, Z. Shuai, H. Zhang, and W. Zhao, "Path following control of autonomous four-wheel-independent-drive electric vehicles via second-order sliding mode and nonlinear disturbance observer techniques," *IEEE Transactions on Industrial Electronics*, vol. 29, p. 1, 2020.

[6] R. K. Subroto, C. Z. Wang, and K. L. Lian, "Four-wheel independent drive electric vehicle stability control using novel adaptive sliding mode control," *IEEE Transactions on Industry Applications*, vol. 56, no. 5, pp. 5995–6006, 2020.

[7] H. Zhang and J. Wang, "Active steering actuator fault detection for an automatically-steered electric ground vehicle," *IEEE Transactions on Vehicular Technology*, vol. 66, no. 5, pp. 3685–3702, 2017.

[8] A.-T. Nguyen, C. Sentouh, and J.-C. Popieul, "Driver-automation cooperative approach for shared steering control under multiple system constraints: design and experiments," *IEEE Transactions on Industrial Electronics*, vol. 64, no. 5, pp. 3819–3830, 2017.

[9] A.-T. Nguyen, C. Sentouh, H. Zhang, and J.-C. Popieul, "Fuzzy static output feedback control for path following of autonomous vehicles with transient performance improvements," *IEEE Transactions on Intelligent Transportation Systems*, vol. 21, no. 7, pp. 3069–3079, 2020.

[10] Z. Zhang, X. Zhang, H. Pan et al., "A novel steering system for a space-saving 4WS4WD electric vehicle: design, modeling, and road tests," *IEEE Transactions on Intelligent Transportation Systems*, vol. 18, no. 1, pp. 114–127, 2017.

[11] M. Schwartz, F. Siebenrock, and S. Hohmann, "Model predictive control allocation of an over-actuated electric vehicle with single wheel actuators," *IFAC-PapersOnLine*, vol. 52, no. 8, pp. 162–169, 2019.

[12] M. F. Selekwa and J. R. Nistler, "Path tracking control of four wheel independently steered ground robotic vehicles," in *Proceedings of the 2011 50th IEEE Conference on Decision and Control and European Control Conference*, pp. 6355–6360, Orlando, FL, USA, December 2011.

[13] E. Maalouf, M. Saad, and H. Saliah, "A higher level path tracking controller for a four-wheel differentially steered mobile robot," *Robotics and Autonomous Systems*, vol. 54, no. 1, pp. 23–33, 2006.

[14] M. Udengaard and K. Iagnemma, "Kinematic analysis and control of an omnidirectional mobile robot in rough terrain," in *Proceedings of the 2007 IEEE/RSJ International Conference on Intelligent Robots and Systems*, pp. 795–800, San Diego, CL, USA, November 2007.

[15] R. Oftadeh, M. M. Aref, R. Ghabcheloo, and J. Mattila, "Bounded-velocity motion control of four wheel steered mobile robots," in *Proceedings of the 2013 IEEE/ASME International Conference on Advanced Intelligent Mechatronics*, pp. 255–260, Wollongong, Australia, July 2013.

[16] F. Fahimi, "Full drive-by-wire dynamic control for four-wheel-steer all-wheel-drive vehicles," *Vehicle System Dynamics*, vol. 51, no. 3, pp. 360–376, 2013.

[17] P. Dai and J. Katupitiya, "Force control for path following of a 4WS4WD vehicle by the integration of PSO and SMC," *Vehicle System Dynamics*, vol. 56, no. 11, pp. 1682–1716, 2018.

[18] Y. Liang, Y. Li, Y. Yu, and L. Zheng, "Integrated lateral control for 4WID/4WIS vehicle in high-speed condition considering the magnitude of steering," *Vehicle System Dynamics*, vol. 58, no. 11, pp. 1711–1735, 2020.

[19] S.-T. Peng, "On one approach to constraining the combined wheel slip in the autonomous control of a 4WS4WD vehicle," *IEEE Transactions on Control Systems Technology*, vol. 15, no. 1, pp. 168–175, 2007.

[20] R. Potluri and A. K. Singh, "Path-tracking control of an autonomous 4WS4WD electric vehicle using its natural feedback loops," *IEEE Transactions on Control Systems Technology*, vol. 23, no. 5, pp. 2053–2062, 2015.

[21] H. Yang, V. Cocquempot, and B. Jiang, "Optimal fault-tolerant path-tracking control for 4WS4WD electric vehicles,"

IEEE Transactions on Intelligent Transportation Systems, vol. 11, no. 1, pp. 237–243, 2010.

[22] M.-H. Lee and T.-H. S. Li, "Kinematics, dynamics and control design of 4WIS4WID mobile robots," *The Journal of Engineering*, vol. 2015, no. 1, pp. 6–16, 2015.

[23] D.-Y. Li, Y.-D. Song, D. Huang, and H.-N. Chen, "Model-independent adaptive fault-tolerant output tracking control of 4WS4WD road vehicles," *IEEE Transactions on Intelligent Transportation Systems*, vol. 14, no. 1, pp. 169–179, 2013.

[24] C. Hu, R. Wang, Z. Wang, M. Chadli, and F. Yan, "Integrated optimal dynamics control of 4WS4WD electric ground vehicles with tire-road frictional coefficient estimation," in *Proceedings of the 2015 American Control Conference (ACC)*, pp. 5426–5431, Hilton Palmer House, CA, USA, July 2015.

[25] C. Hu, R. Wang, and F. Yan, "Integral sliding mode-based composite nonlinear feedback control for path following of four-wheel independently actuated autonomous vehicles," *IEEE Transactions on Transportation Electrification*, vol. 2, no. 2, pp. 221–230, 2016.

[26] W. Kim, D. Kim, K. Yi, and H. J. Kim, "Development of a path-tracking control system based on model predictive control using infrastructure sensors," *Vehicle System Dynamics*, vol. 50, no. 6, pp. 1001–1023, 2012.

[27] H. Alipour, M. B. Bannae Sharifian, and M. Sabahi, "A modified integral sliding mode control to lateral stabilisation of 4-wheel independent drive electric vehicles," *Vehicle System Dynamics*, vol. 52, no. 12, pp. 1584–1606, 2014.

[28] H. Park and J. C. Gerdes, "Optimal tire force allocation for trajectory tracking with an over-actuated vehicle," in *Proceedings of the 2015 IEEE Intelligent Vehicles Symposium (IV)*, pp. 1032–1037, Seoul, South Korea, July 2015.

[29] V. Nazari and M. Naraghi, "A vision-based intelligent path following control of a four-wheel differentially driven skid steer mobile robot," in *Proceedings of the 2008 10th International Conference on Control, Automation, Robotics and Vision*, pp. 378–383, Hanoi, Vietnam, December 2008.

[30] S. Wagner, S. Zipser, R. Bartholomaeus, and B. Bernard, "A novel two dof control for train-like guidance of multiple articulated vehicles," 2009.